(1987)]; electrophysiology was performed as detailed (*13*).

18. M. Hollmann *et al.*, *Cold Spring Harbor Symp. Quant. Biol.*, in press.
19. The hippocampal poly(A$^+$) RNA (Figs. 2 and 3) was extracted from adult rat brain hippocampus and is, therefore, derived from a complex mixture of neuronal and non-neuronal cell types, each of which may express some GluR subunit RNAs and not others. The hippocampal RNA may also contain, in addition to GluR1, GluR2, and GluR3 RNAs, transcripts encoding as yet uncharacterized GluR subunits or proteins that can modulate glutamate receptor responses. Therefore, the data obtained with hippocampal RNA must be considered as a composite response of all expressed, functional glutamate receptors. Furthermore, the bringing together of inappropriate types, numbers, or combinations of GluR subunits in a single oocyte may result in receptors having an uncertain physiological relevance. The precise relationship, then, between bona fide glutamate receptors in neurons and the responses in oocytes injected with hippocampal poly(A$^+$) RNA remains to be established.
20. C. Hirono, I. Ito, S. Yamagishi, H. Sugiyama, *Neurosci. Res.* **6**, 106 (1988); T. A. Verdoorn and R. Dingledine, *Mol. Pharmacol.* **34**, 298 (1988); T. A. Verdoorn *et al.*, *ibid.* **35**, 360 (1989).
21. In situ hybridization histochemistry was performed as described [E. S. Deneris, J. Boulter, L. W. Swanson, J. Patrick, S. Heinemann, *J. Biol. Chem.* **264**, 6268 (1989)] with [^{35}S]antisense RNA probes and 30-μm-thick paraformaldehyde-fixed coronal sections of adult rat brains. Antisense RNA was prepared from full-length plasmid clones p59/2 (GluR1), pRB14 (GluR2), and pRB312 (GluR3). Sections were exposed to DuPont Cronex film for 10 days. To assess specificity, a second set of hybridizations was performed with short (600 to 900 nt) antisense probes from untranslated regions or from areas of minimal nucleotide sequence homology. The hybridization patterns were identical for both sets of probes.
22. E. S. Deneris, unpublished data.
23. B. Bettler *et al.*, manuscript in preparation.
24. M. Hollmann, unpublished data.
25. N. I. Kiskin *et al.*, *Neurosci. Lett.* **63**, 225 (1986); T. A. Verdoorn and R. Dingledine, *Mol. Pharmacol.* **34**, 289 (1988); C. F. Zorumski and J. Yang, *J. Neurosci.* **8**, 4277 (1988); J.-P. Pin, B. J. Van Vliet, J. Bockaert, *Eur. J. Pharmacol.* **172**, 81 (1989).
26. M. Iino, S. Ozawa, K. Tsuzuki, *J. Physiol. (London)* **424**, 151 (1990).
27. J. Steinbach and C. Ifune, *Trends Neurosci.* **12**, 3 (1989).
28. K. Keinänen *et al.*, *Science* **249**, 556 (1990).
29. J. Devereux, P. Haeberli, O. Smithies, *Nucleic Acid Res.* **12**, 387 (1984).

30. We thank B. Bettler, I. Hermans-Borgmeyer, R. Duvoisin, and R. Papke for advice and comments during the preparation of this manuscript. Supported in part by postdoctoral fellowships from the National Institutes of Health (E.S.D.) and the Deutsche Forschungsgemeinschaft (M.H.) and grants from the Muscular Dystrophy Association, NIH (NS11549 and NS28709) and the Fritz B. Burns Foundation (S.H.).

23 July 1990; accepted 10 August 1990

Stereoscopic Depth Discrimination in the Visual Cortex: Neurons Ideally Suited as Disparity Detectors

IZUMI OHZAWA,* GREGORY C. DEANGELIS, RALPH D. FREEMAN

The possibility has been explored that a subset of physiologically identifiable cells in the visual cortex is especially suited for the processing of stereoscopic depth information. First, characteristics of a disparity detector that would be useful for such processing were outlined. Then, a method was devised by which detailed binocular response data were obtained from cortical cells. In addition, a model of the disparity detector was developed that includes a plausible hierarchical arrangement of cortical cells. Data from the cells compare well with the requirements for the archetypal disparity detector and are in excellent agreement with the predictions of the model. These results demonstrate that a specific type of cortical neuron exhibits the desired characteristics of a disparity detector.

THE NEURAL PROCESS OF STEREOscopic depth discrimination is thought to be initiated in the visual cortex. However, the mechanisms of this neural process are not clear (*1*). One fundamental question concerns the roles of specific cell types in the processing of information concerning stereoscopic depth. The two major subdivisions of cortical cells, as determined physiologically, are "simple" and "complex." Simple cells have receptive fields (RFs) that consist of spatially separate subregions that respond to either onset or offset of a flashed stationary bar of light (ON or OFF responses). Alternatively, a bar stimulus that is brighter or darker than the background may be used to classify a simple cell (Fig. 1A) (*2*). Complex cells, on the other hand, respond to a stimulus anywhere within the RF for both bright and dark bars (Fig. 1B). Complex cells, therefore, are insensitive to contrast polarity, that is, whether the stimulus is darker or brighter than the background, and are only broadly selective to stimulus position. Upon cursory analysis, these monocular characteristics of complex cells appear inappropriate for fine stereoscopic depth discrimination because precise position and contrast information are not available. However, the study of binocular properties of these cells, reported here, demonstrates that a proportion of complex cells is especially suited as fine binocular disparity sensors (*3*). A model of this sensor provides quantitative predictions that may be compared with responses of cells.

What additional binocular properties of complex cells are required in order to create a suitable disparity detector? First, the disparity selectivity of complex cells must be much finer than that predicted by the size of the RFs (*4*). Second, the preferred disparity must be constant for all stimulus positions within the RF. Third, incorrect contrast polarity combinations should be ineffective if presented at the optimal disparity for the matched polarity pair, that is, a combination of a bright bar to one eye and a dark bar to the other should not elicit a response at the preferred disparity of the detector.

The first two requirements are illustrated in Fig. 2. In Fig. 2A, a cross-sectional view is shown of the plane containing the two eyes and the RFs. The RF of a cortical neuron is depicted in image space on left eye and right eye retinas. When extended into object space, the intersections between left and right RF projections define the region that is "viewed" by the cell through both eyes (hatched, diamond-shaped zone). Planes of constant disparities are indicated by horizontal lines for uncrossed (positive) and crossed (negative) disparities. If a neuron simply detects the simultaneous presence of a stimulus within both left eye and right eye RFs, any stimulus that falls within the diamond-shaped zone will excite the cell. Because this region spans a wide range of binocular disparities, the neuron is limited to crude disparity sensitivity. A disparity detector must respond to a much more restricted range of visual space. In this case, the dark shaded oval region around zero disparity represents a suitable zone.

A graphical depiction of this region is shown in Fig. 2B. Stimulus positions along the left eye and right eye RFs are represented on the x_L and x_R axes, respectively. The diagonal slope represents a plane of constant (zero) disparity. As in Fig. 2A, a region of visual space is defined (hatched square) within which left eye and right eye RFs are jointly stimulated. The dark shaded area corresponding to the oval in the upper part of the figure is shown along the diagonal, which represents zero disparity. Again, this latter zone represents the narrow response range of our disparity detector tuned to a

Groups in Neurobiology and Bioengineering, School of Optometry, University of California, Berkeley, CA 94720.

*To whom correspondence should be addressed.

constant disparity. For nonzero disparity, the sensitive region for a detector must be located parallel to and off the diagonal.

The third requirement concerns matching of contrast polarity. The archetypal disparity detector should respond to stimuli delivered to both eyes at the preferred disparity, provided that contrast polarity is the same. Thus, a matched pair of bright or dark bars with correct disparity should yield a vigorous response. However, the detector should not be activated if contrast polarities of the bars are different in the two eyes because such a difference cannot arise from the same part of a binocularly viewed object. This is a nontrivial requirement because, monocularly, complex cells respond similarly to bright or dark bars within the RF. It is therefore counterintuitive to expect the detector to reject a pair of bars at the correct disparity on the basis of mismatched contrast polarity (*5*).

We have conducted tests of neurons in the cat's visual cortex in order to determine if the cells in a biological system fulfill the requirements for the disparity detector outlined above (*6*). Once extracellularly recorded action potentials from a cell are isolated and RFs are located, initial tests are performed with moving grating stimuli that consist of alternating black and white stripes with sinusoidal luminance distribution across the bars. We found the optimal monoptic parameters of the grating by measuring the neuron's discharge rate to different values of orientation and spatial frequency. We determined the sensitivity to binocular disparity by presenting gratings dichoptically at a variety of relative phases. These and other standard tests were used to classify each cell as simple or complex and to establish if the neuron was disparity-selective (*7*). To compare responses of cells with those of the archetypal detector, we obtained detailed binocular interaction profiles with respect to positions and contrast polarities of stimuli for the two eyes. We used a binocular version of a reverse correlation technique that provides a rapid and quantitative method of mapping these profiles (*8*). In this procedure, a bar of optimal orientation is presented to each eye simultaneously for 50 ms. For each eye, position and contrast polarity of the bar are randomized, and different stimuli are presented in successive flashes. To cover all possible left-right combinations of stimuli, the stimulus set is constructed so that it forms a two-dimensional array of points covering the hatched square of Fig. 2B. After the procedure has been repeated with different randomized stimulus sets, complete disparity selectivity profiles are obtained as four two-dimensional histograms, one for each permutation of contrast pairs.

Results have been obtained for 79 cortical cells, of which 40 are simple and 39 are complex. Findings for representative cells are shown in Fig. 3A. For the simple cell (top row of panels), disparity selectivity profiles are shown for all four combinations of bright and dark bars for the two eyes. For the matched pairs (left two panels in this row), clear complementary patterns are seen for bright and dark pair responses. Clearly, both position and contrast polarity critically affect the response profile. These binocular response profiles for the simple cell are easily predicted from the one-dimensional monocular RF profiles shown at the bottom and left margins of each panel (*9*). Similar complementary profiles are also observed for the mismatched contrast pairs (right two panels in this row) (*10*).

Consider next the results for a complex cell (Fig. 3A, second row). The two panels on the left represent response profiles obtained with matched contrast pairs (two dark or two bright bars). Note the similarity of these profiles to the desired behavior of the archetypal detector in Fig. 2B (*11*). Elongated response contours are seen along the diagonal, indicating that the disparity selectivity is much narrower than the extent of the RFs. The contours also indicate that the preferred disparity is constant and independent of stimulus position within the fields. Results for pairs of matched bars (two dark or two bright) show similar patterns, indicating that response is independent of contrast polarity. In both cases of mismatched contrast polarity pairs (right two panels of the second row), the disparity along the diagonal, which is most effective for the matched contrast pairs, is ineffective in that there is a clear lack of response. The disparity selectivity profile for this condition

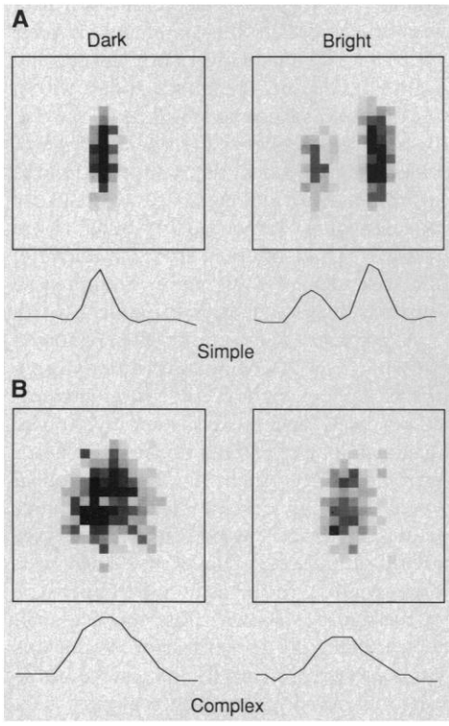

Fig. 1. Two-dimensional RFs of representative neurons in the primary visual cortex. Each panel represents a square area (5° by 5°) slightly larger than an RF. The area is oriented to match the preferred orientation of each neuron. An array of 20 by 20 locations is used to estimate local responsivity for dark and bright bars. The darker a point in each panel, the more likely the cell is to fire when stimulated with an appropriate bar at this location. The curve below each panel shows a one-dimensional RF profile obtained by integrating the corresponding two-dimensional profile along the *y* axis. (**A**) Simple cell RFs are shown for dark and bright bar stimuli on left and right sides, respectively. Note that the dark and bright stimuli cause responses in spatially separate elongated subregions. The square area and the stimulus bars are oriented 10° from vertical. The dimensions of the stimulus bar are 2° by 0.5° (**B**) Complex cell RFs. Both bright and dark bars excite the neuron in the same general area within the RFs. In addition, no elongated subregions are observed. The square area and the stimuli are oriented 15° from vertical. The stimulus dimensions are 1.5° by 0.5°.

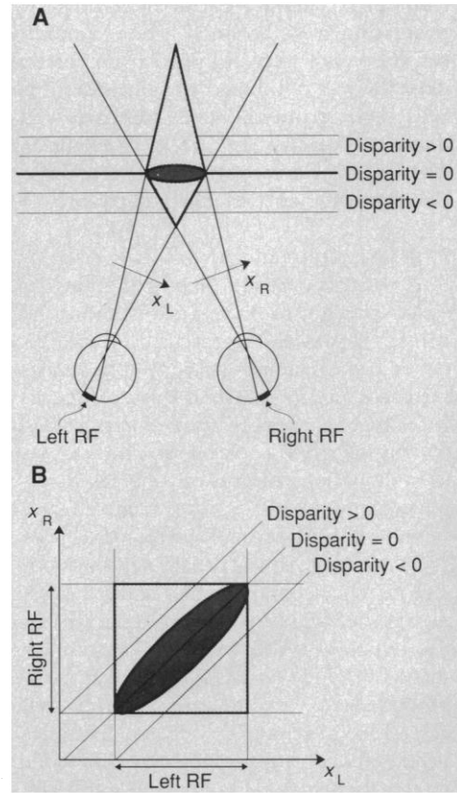

Fig. 2. Characteristics required for an archetypal disparity detector. (**A**) Geometry of a binocular viewing condition as viewed from above. (**B**) The requirements for a disparity detector are shown with Cartesian coordinates where axes represent positions along left and right RFs.

is complementary to that of the matched contrast pair, and there are two excitatory contours that run parallel to the diagonal. This indicates that the preferred disparity for the mismatched contrast pair has a different value than that for the matched pair. These findings show that the complex cell rejects mismatched contrast polarities at the disparity that is optimal for the matched condition. Similar data from another complex cell are shown in the third row of Fig. 3A, and one sees the same basic features as those described above. Considered together, the properties of the complex cells illustrated here fulfill all three requirements for the disparity detector.

Response characteristics for the cells described above are typical of what we have observed. Although there are individual variations, all of the simple cells we have recorded follow the patterns of the example

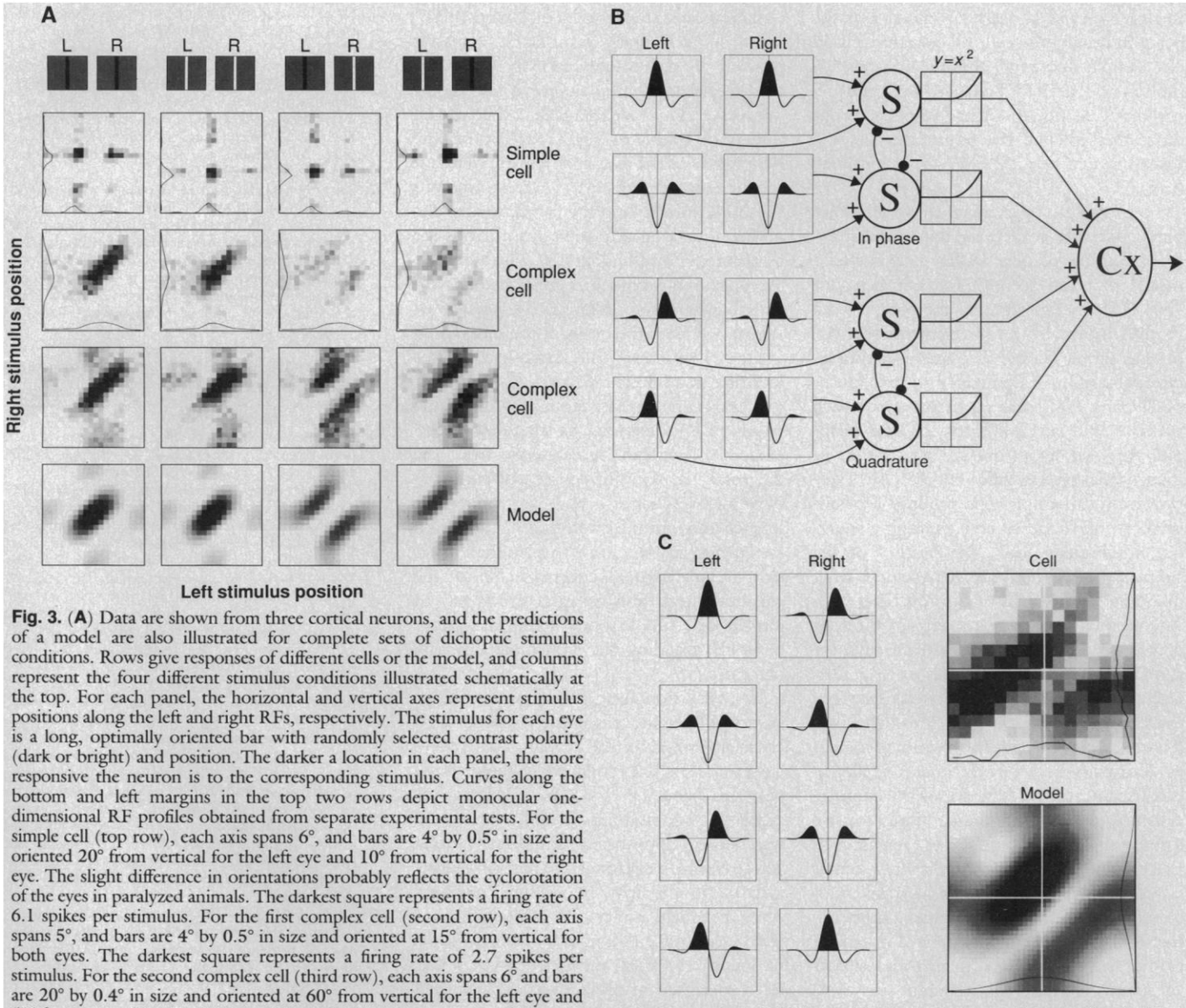

Fig. 3. (**A**) Data are shown from three cortical neurons, and the predictions of a model are also illustrated for complete sets of dichoptic stimulus conditions. Rows give responses of different cells or the model, and columns represent the four different stimulus conditions illustrated schematically at the top. For each panel, the horizontal and vertical axes represent stimulus positions along the left and right RFs, respectively. The stimulus for each eye is a long, optimally oriented bar with randomly selected contrast polarity (dark or bright) and position. The darker a location in each panel, the more responsive the neuron is to the corresponding stimulus. Curves along the bottom and left margins in the top two rows depict monocular one-dimensional RF profiles obtained from separate experimental tests. For the simple cell (top row), each axis spans 6°, and bars are 4° by 0.5° in size and oriented 20° from vertical for the left eye and 10° from vertical for the right eye. The slight difference in orientations probably reflects the cyclorotation of the eyes in paralyzed animals. The darkest square represents a firing rate of 6.1 spikes per stimulus. For the first complex cell (second row), each axis spans 5°, and bars are 4° by 0.5° in size and oriented at 15° from vertical for both eyes. The darkest square represents a firing rate of 2.7 spikes per stimulus. For the second complex cell (third row), each axis spans 6° and bars are 20° by 0.4° in size and oriented at 60° from vertical for the left eye and 50° from vertical for the right eye. The darkest square represents a firing rate of 4.1 spikes per stimulus. The prediction of the model (bottom row) plots the function

$$R(x_L, x_R) = \{[\exp(-kx_L^2)\cos 2\pi x_L + \exp(-kx_R^2)\cos 2\pi x_R]^2 + [\exp(-kx_L^2)\sin 2\pi x_L + \exp(-kx_R^2)\sin 2\pi x_R]^2\}^{1/2}$$

where $k = 5.5$ and x_L and x_R are left and right stimulus positions, respectively. (**B**) A model of a complex cell (Cx) that fulfills requirements for the archetypal disparity detector is shown, in which the complex cell receives input from a minimum of four simple-type subunits (S). The simple-type subunits within each pair are mutually inhibitory, as indicated by reciprocal connections between the top two and bottom two units. This inhibitory pathway is essential to provide spatial antagonism to RF flanks. The quadrature phase relation is depicted by the 90° phase difference between the RF profiles of the two pairs as shown in insets at the left of the simple-type subunits. The positive parts of each profile (filled areas) may be interpreted as the spatial distribution of excitatory inputs from ON-center lateral geniculate nucleus (LGN) cells. The negative parts of the profiles (unfilled areas) represent the distribution of excitatory inputs from OFF-center LGN neurons. Note that mutual inhibition will not be activated simultaneously in both directions for a bar stimulus because input distributions are complementary. Nonlinearity is an additional requirement because simple cells typically show no spontaneous discharge, and they therefore cannot signal inhibition. In the insets for the nonlinearities, a positive input represents excitation of the simple cell, and a negative value denotes inhibition. (**C**) Responses are shown of a complex cell and a model with asymmetric disparity tuning profiles. The insets at the left show RF profiles of four subunits that have a "double quadrature" organization in which the quadrature relation applies to RF profiles between the eyes as well as between subunit pairs. Curves (black) in the two panels at the right show monocular RF profiles. The cross hairs (white) show peaks of these profiles. For the complex cell shown, each axis spans 7°, and the bars are 20° by 0.4° and oriented at 50° from vertical for the left eye and 40° from vertical for the right eye. Responses are shown to dark bars in both eyes. The darkest square represents a firing rate of 3.1 spikes per stimulus.

in Fig. 3A. With respect to complex cells, the response patterns described above are found mainly in a subset of cells that meets two conditions. First, they exhibit disparity (phase) selectivity to dichoptically presented sinusoidal gratings. In our current study, 51% of complex cells showed disparity selectivity. Second, they are highly binocular in that each eye is nearly as effective as the other in driving the cell. All complex cells in our sample that fulfill these conditions exhibited the desired behavior (*12*). Of 39 complex cells tested, 15 had response properties that fulfilled the requirements for a disparity detector that we have outlined here.

To propose a mechanism by which complex cells might achieve the required disparity sensing properties, we have developed a model that can account for this behavior (Fig. 3B). In this scheme, the complex cell receives inputs from four elements that behave as simple cells (*13*). These four simple-type subunits are organized into two "push-pull" pairs (*14*), that is, members of each pair are mutually inhibitory. These push-pull pairs are in quadrature phase, that is, their spatial phases differ by 90° (*15*). Outputs from the simple-type subunits are half-wave–rectified and emerge through a squaring nonlinearity (*16*). RF profiles of the simple-type subunits are represented schematically to the left by Gabor functions (*17*). The predictions of this model, for the four contrast conditions used to test the cells, are shown in the bottom panels of Fig. 3A. Column by column comparisons between the predictions of the model and the data from the complex cells show striking matches. Although there may be other models that can account for the behavior of the complex cells described above, the configuration we suggest in Fig. 3B requires the fewest subunits and is plausible because it incorporates a well-established hierarchical cortical architecture. The model thus provides a quantitative foundation for a hierarchical organization of the visual cortex, in that the outputs of specific simple-type subunits are combined to produce a complex cell receptive field.

Simple cells are also selective to binocular disparity. However, they do not encode disparity information exclusively because they are also selective for position and contrast polarity, spatial frequency, and orientation. In this sense, a simple cell is a sensor for a multitude of stimulus parameters. On the other hand, complex cells encode disparity information independently of position and contrast polarity. Such invariant properties are advantageous for a detector because responses are not affected by changes in irrelevant parameters.

How do our results relate to the traditional notion of the neural basis of stereoscopic depth discrimination? Consider the symmetry of profiles about the diagonal for the complex cell data shown in Fig. 3A. According to the traditional view, this would be classed as "tuned excitatory" because of the symmetry about zero disparity (*18*). This classification system also incorporates "near" and "far" cells with asymmetric disparity profiles. We also found neurons with asymmetric tuning profiles, as shown for a complex cell and a model (Fig. 3C). The model is identical to that of Fig. 3B except that the RF profiles of the four subunits are different for the left and right eyes (Fig. 3C, insets). For both the data and the predictions of the model, the elongated excitatory regions are not centered on the diagonal. Furthermore, the maximum binocular response is obtained when the stimulus is positioned slightly off from the peaks of the monocular excitatory profiles (white cross-hairs). This indicates that selectivity to a nonzero disparity does not necessarily require lateral spatial offsets of RF positions, as suggested previously (*1*), but can instead arise from the difference in RF profiles of subunits between left and right eyes. The primary difference between the traditional classification system and our scheme is that, in the former case, no special distinction is made for the roles of simple and complex cell types. In our model, simple units serve as components for building the archetypal disparity detectors (*19*).

In conclusion, our results show that a subset of complex cells in the visual cortex is especially suited for the detection of binocular disparities. The model we propose shows that this behavior of complex cells can be achieved by combining outputs from a small number of appropriate simple-type RFs. These complex cells must be part of a larger system of disparity processing neurons. Note that the complex cells we have studied also carry information concerning spatial frequency (or size) and orientation, a fact not considered in previous neural explanations of disparity selectivity. One way in which all of these response properties can be integrated is by encoding binocular disparity information in the visual cortex at a number of different size or spatial frequency scales (*1*). Complex cells at each scale can signal disparity information with a range and accuracy commensurate with their selectivity to size or spatial frequency. This scheme, therefore, enables a unification of monocular image and binocular disparity representations.

REFERENCES AND NOTES

1. The standard notion is that cortical cells are sensitive to different disparities by virtue of lateral shifts of RFs [H. B. Barlow, C. Blakemore, J. D. Pettigrew, *J. Physiol. (London)* **193**, 327 (1967); R. von der Heydt, C. S. Adorjani, P. Hänny, G. Baumgartner, *Exp. Brain Res.* **31**, 523 (1978); R. Maske, S. Yamane, P. O. Bishop, *Vision Res.* **24**, 1921 (1984)]. An alternative view is that binocular disparities are processed at a number of different size or spatial frequency scales [D. Marr and T. Poggio, *Proc. R. Soc. London Ser. B* **204**, 301 (1979)]. Other models of binocular disparity detection have been proposed in which phase components of Gabor-filtered left-right images are used as matching primitives [T. D. Sanger, *Biol. Cybern.* **59**, 405 (1988); M. Jenkin and A. D. Jepson, in *Computational Processes in Human Vision*, Z. Pylyshyn, Ed. (Ablex, Norwood, NJ, 1988), pp. 69–98]. In more physiologically plausible models, binocular RFs encode disparity as phase while maintaining retinal correspondence [R. D. Freeman and I. Ohzawa, *Vision Res.*, in press; M. Nomura, G. Matsumoto, S. Fujiwara, *Biol. Cybern.* **63**, 237 (1990)].
2. The original definitions of simple and complex cells [D. H. Hubel and T. N. Wiesel, *J. Physiol. (London)* **160**, 106 (1962)] may be expanded to include responses to bar-shaped stimuli that are brighter or darker than the background. For simple cells, an approximate correspondence exists between ON/OFF areas and bright/dark areas, respectively [R. Maske, S. Yamane, P. O. Bishop, *J. Neurophysiol.* **53**, 670 (1985); see (*8*)].
3. A previous finding that only complex cells respond to dynamic random-dot stereograms also suggests a special role for these cells in stereopsis [G. F. Poggio, B. C. Motter, S. Squatrito, Y. Trotter, *Vision Res.* **25**, 397 (1985)].
4. This behavior of disparity-selective complex cells has been reported [T. Nikara, P. O. Bishop, J. D. Pettigrew, *Exp. Brain Res.* **6**, 353 (1968)].
5. Detailed monoptic examinations of complex RFs with two bar-shaped stimuli reveal internal structures of these RFs [J. A. Movshon, I. D. Thompson, D. J. Tolhurst, *J. Physiol. (London)* **283**, 79 (1978); R. G. Szulborski and L. A. Palmer, *Vision Res.* **30**, 249 (1990)]. Responses depend on the relative position and the contrast polarities of the two stimuli.
6. Animals were anesthetized with halothane (3% in O_2) during surgery. During recordings, cats were paralyzed with gallamine triethiodide that was infused continuously at the rate of 10 mg kg^{-1} $hour^{-1}$. Sodium thiamylal (Surital) was also infused at the rate of 1 mg kg^{-1} $hour^{-1}$. Artificial respiration was carried out with a gas mixture of N_2O, O_2, and CO_2 (70%:29%:1%). A microelectrode was lowered into visual cortex through a closed chamber, and action potentials from single neurons were recorded with 1-ms resolution. Visual stimuli were presented dichoptically on a pair of cathode ray tube displays (mean luminance, 50 cd m^{-2}). Details of these methods and procedures have been reported [I. Ohzawa and R. D. Freeman, *J. Neurophysiol.* **56**, 221 (1986)].
7. Simple cells exhibit a highly modulated discharge at the temporal frequency of the drifting grating. Complex cells respond with an overall increase in average discharge rate. A disparity-selective cell changes its rate of discharge as relative phase is varied between dichoptically presented sinusoidal gratings.
8. In the reverse correlation method, a causal relation between stimulus and response is sought in the reverse direction of time. Rather than measure responses after the onset of a stimulus in the forward direction of time, one correlates each action potential backward in time to the most likely causal stimulus in the recent past. For the measurement of RF profiles, the stimulus presented on the screen 30 to 60 ms before the spike occurrence is identified. The optimal time delay varies from one cell to another, presumably reflecting the visual latency of the neuron. Each occurrence of a spike increments a histogram bin corresponding to the causal stimulus. The resulting two-dimensional histograms represent RF profiles of the neuron [J. P. Jones and L. A. Palmer, *J. Neurophysiol.* **58**, 1187 (1987)]. In the binocular version of this method, two monitor displays are used dichoptically. A bar is presented on each display simultaneously, in various combinations of contrast polarity and position. The same

reverse correlation algorithm is used to identify the stimulus and hence to select a histogram bin to increment, except that the stimulus now consists of a pair of bars for the two eyes.

9. D. Ferster, *J. Physiol. (London)* **311**, 623 (1981).
10. Disparity tuning curves in all earlier studies have been obtained by sweeping a pair of bars with varying binocular disparities over the RFs. Such tuning curves may be predicted from our data by integrating the two-dimensional profiles of Fig. 3A along the constant disparity lines parallel to the 45° diagonal.
11. We cannot determine whether the elongated diagonal contours in Fig. 3A lie at zero disparity.
12. It is of interest to determine if there is a correlation between the preferred orientations of complex cells and the behavior of these neurons as disparity detectors. We have observed desired behavior for cells with a wide variety of preferred orientations. Our sample size is not currently sufficient to permit conclusions to be drawn in this regard.
13. Our model is a binocular generalization of a model proposed previously [D. A. Pollen and R. F. Ronner, *Vision Res.* **22**, 101 (1982); *IEEE Trans. Sys. Man Cybern.* **13**, 907 (1983); D. A. Pollen, J. P. Gaska, L. D. Jacobson, in *Models of Brain Function*, R. M. J. Cotterill, Ed. (Cambridge Univ. Press, Cambridge, 1989), p. 115].
14. D. Ferster, *J. Neurosci.* **8**, 1172 (1988); R. A. Stepnoski and L. A. Palmer, *Invest. Ophthalmol. Vis. Sci.* **30** (suppl.), 297 (1989); K. H. Foster *et al.*, *J. Physiol. (London)* **345**, 22P (1983).
15. Nearby simple cell pairs, recorded from a single electrode, show response phase differences of 90°, suggesting a quadrature relation of the pairs [D. A. Pollen and S. F. Ronner, *Science* **212**, 1409 (1981)].
16. Combining squared outputs of quadrature subunits provides smooth profiles for complex cell RFs. Such schemes are called "energy models" and were first used to describe mechanisms of motion perception [E. H. Adelson and J. R. Bergen, *J. Opt. Soc. Am.* **A2**, 284 (1985); R. C. Emerson, M. J. Korenberg, M. C. Citron, in *Advanced Methods of Physiological System Modeling*, V. Z. Marmarelis, Ed. (Plenum, New York, 1989), vol. 2, p. 97]. Our model, therefore, is an energy model of disparity detection.
17. A Gabor function is the product of a Gaussian and a sinusoid [D. Gabor, *J. Inst. Electr. Eng.* **93**, 429 (1946)]. The use of one-dimensional Gabor functions as RF profiles (Fig. 3B, insets) is consistent with two-dimensional models of simple-cell RFs proposed previously [J. Marcelja, *J. Opt. Soc. Am.* **70**, 1297 (1980); J. G. Daugman, *ibid.* **A2**, 1160 (1985); J. P. Jones and L. A. Palmer, *J. Neurophysiol.* **58**, 1233 (1987)]. This is because the one-dimensional RF as measured by a thin, long bar stimulus of optimal orientation, is given by the integral of the two-dimensional Gabor profile along the length of RF flanks. This integral, as shown below, is also a Gabor function with the same extent and spatial frequency as the two-dimensional function.

$$\int_{-\infty}^{\infty} G(x, y)dy = \int_{-\infty}^{\infty} \exp(-\alpha x^2 - \beta y^2)$$
$$\cos(2\pi fx + \theta)dy = A \exp(-\alpha x^2)\cos(2\pi fx + \theta)$$

where α and β are constants, f is the frequency, θ is the phase, and A is an integration constant. It is not necessary for the model to have even an odd symmetry for the RFs of quadrature pairs. Therefore, the model does not conflict with a previous finding that simple RF profiles are not generally even or odd symmetric [D. J. Field and D. J. Tolhurst, *Proc. R. Soc. London Ser. B* **228**, 379 (1986)].
18. G. F. Poggio and B. Fischer, *J. Neurophysiol.* **40**, 1392 (1977).
19. In the classification scheme of Poggio and Fischer (*18*), all categories are defined with respect to absolute disparity, whereas our system is defined in terms of phase at each spatial frequency scale. This difference is probably the reason why the former scheme needed the addition of two new categories (tuned-near, tuned-far) to the original four [G. F. Poggio *et al.*, *J. Neurosci.* **8**, 4531 (1988)].
20. Supported by NIH grant EY01175. We thank G. Ghose for help with the experiments and detailed review of the manuscript.

14 February 1990; accepted 8 June 1990

Activation of Extrastriate and Frontal Cortical Areas by Visual Words and Word-Like Stimuli

STEVEN E. PETERSEN, PETER T. FOX,* ABRAHAM Z. SNYDER, MARCUS E. RAICHLE

Visual presentation of words activates extrastriate regions of the occipital lobes of the brain. When analyzed by positron emission tomography (PET), certain areas in the left, medial extrastriate visual cortex were activated by visually presented pseudowords that obey English spelling rules, as well as by actual words. These areas were not activated by nonsense strings of letters or letter-like forms. Thus visual word form computations are based on learned distinctions between words and nonwords. In addition, during passive presentation of words, but not pseudowords, activation occurred in a left frontal area that is related to semantic processing. These findings support distinctions made in cognitive psychology and computational modeling between high-level visual and semantic computations on single words and describe the anatomy that may underlie these distinctions.

STUDIES IN COGNITIVE PSYCHOLOGY (*1–3*) and neurology (*4*) have supported the idea that there are complex computations made on words and word-like letter strings that link the visual input into a unit. For example, each letter of a word can be perceived at a lower threshold than when that letter is presented alone or as part of a nonsense string of letters (*3*). This perceptual advantage extends to pseudowords, meaningless letter strings that are similar to words (for example, POLT), but not to random strings of letters (for example, PXQLO) suggesting that this effect does not involve the meaning of the string but its regularity, that is, its similarity to strings of letters that would be words (*5*).

In an earlier study of single word processing, we showed that passively presented visual words activated a number of extrastriate areas bilaterally in the occipital lobes (*6*). In that study, only words were used as stimuli, thus there was no evidence that these activations were unique to words. Additionally, when subjects were required to generate the meaning of visual or auditory words, or to monitor a list of words for a semantic category, an area of the left prefrontal cortex was active, suggesting that this frontal region is related to semantic processing (*6*). In cognitive studies it has often been argued that some lexical and semantic processing is carried out automatically whenever a word is presented (*7*). This processing may involve areas within the left prefrontal cortex (*8*), but there was no evidence of activation of the left frontal area during passive presentation of words (*6*). To explore these issues further, we designed PET experiments to compare the areas activated during the visual representation of four different sets of word-like stimuli.

Subjects were normal volunteers between 18 and 49 years old. All subjects (n = 8, five males and three females) were native English speakers and strongly right-handed. Most subjects were students in the medical, allied health, or graduate schools of Washington University. These people, as a group, were assumed to be normal or above in reading skills and general intelligence.

The PET imaging, general task design, and data analysis strategies have been described and include (i) the use of ^{15}O-labeled water as a blood flow tracer [the short radioactive half-life (123 s) and scan time (40 s) of [^{15}O]H_2O allow eight scans to be done in a single session (*9*)]; (ii) paired (task minus control) image subtraction to isolate areas of change between active and control conditions (*10*); (iii) intersubject image averaging to increase the signal strength of active regions compared to the noise background (*11*); (iv) a two-stage (omnibus and post hoc) statistical analysis to describe the significance of the foci in the averaged subtraction images (*11*).

Seven scans were performed on each subject. A fixation-point-only control scan was obtained while the subject fixated on a blank screen interposed between each of four stimulus-set scans (*12*). The order of presentation of stimulus sets was counterbalanced among individuals, and the order of presentation within sets was pseudorandomized.

S. E. Petersen, Department of Neurology and Neurological Surgery, Department of Anatomy and Neurobiology, Department of Psychology, and the McDonnell Center for Higher Brain Function, Washington University School of Medicine, 660 South Euclid, Box 8111, St. Louis, MO 63110.
P. T. Fox, A. Z. Snyder, M. E. Raichle, Department of Neurology and Neurological Surgery, Department of Radiology, Division of Radiation Science, Mallinckrodt Institute of Radiology, and the McDonnell Center for Higher Brain Function, Washington University School of Medicine, 660 South Euclid, Box 8111, St. Louis, MO 63110.

*Present address: The Johns Hopkins Hospital, Neuroradiology Section, Meyer 8-140, Baltimore, MD 21205.

References and Notes

[1] **A Computational Theory of Human Stereo Vision**

D. Marr; T. Poggio

Proceedings of the Royal Society of London. Series B, Biological Sciences, Vol. 204, No. 1156. (May 23, 1979), pp. 301-328.

Stable URL:

http://links.jstor.org/sici?sici=0080-4649%2819790523%29204%3A1156%3C301%3AACTOHS%3E2.0.CO%3B2-4

[15] **Phase Relationships between Adjacent Simple Cells in the Visual Cortex**

Daniel A. Pollen; Steven F. Ronner

Science, New Series, Vol. 212, No. 4501. (Jun. 19, 1981), pp. 1409-1411.

Stable URL:

http://links.jstor.org/sici?sici=0036-8075%2819810619%293%3A212%3A4501%3C1409%3APRBASC%3E2.0.CO%3B2-6

[17] **The Structure and Symmetry of Simple-Cell Receptive-Field Profiles in the Cat's Visual Cortex**

D. J. Field; D. J. Tolhurst

Proceedings of the Royal Society of London. Series B, Biological Sciences, Vol. 228, No. 1253. (Sep. 22, 1986), pp. 379-400.

Stable URL:

http://links.jstor.org/sici?sici=0080-4649%2819860922%29228%3A1253%3C379%3ATSASOS%3E2.0.CO%3B2-6